RESEARCH PAPER

A harmonic oscillator model of atmospheric dynamics using the Newton-Kepler planetary approach

Alexander Munson [ID] [1,*,‡]

[1]Department of Mathematics, Physics, and Computer Science, Wilson College, PA 17201, United States
*Corresponding Author
‡alexander.munson@wilson.edu (Alexander Munson)

Abstract

Projection of future meteorological patterns such as median temperature and precipitation is necessary for governments to facilitate civil aviation, forecast agricultural productions, and advise public energy policies. Various models are proposed based on historical data, such as the short-term 7-day forecast or the long-term Global Forecast System, to study climate change. The main contribution of the paper is that it gives a feasible, cost-effective model for median-term projections with statistically tested accuracies well within the accepted margins of the scientific community. This model is the starting point to provide general guidelines to governments to forecast levels of energy consumption for residential cooling in summer and heating in winter to provide energy subsidies for low-income populations and for organizations supporting countries needing energy assistance. Additionally, mid-term models are also useful during global energy disruptions. A theoretical model is derived based on orbital mechanics, planetary science, and astronomy using Newton's Law of Universal Gravitation and Kepler's Laws of Planetary Motions. The model is then optimized with historical data in a specific region. The model's predictions are then statistically compared with the actual observed temperature outside the training data. In sum, the current harmonic oscillator method can be beneficially utilized by governments to forecast natural phenomena in order to provide timely assistance to respective populations such as predicting extreme temperature fluctuations in the planning of agricultural productions.

Keywords: Harmonic oscillators; Newton's law of gravitation; Kepler's laws of planetary motion; orbital mechanics

AMS 2020 Classification: 35C07; 35A25; 76A05

1 Introduction

The study of atmospheric phenomena to project weather patterns by mathematical modelling has a long history. The traditional approach has been gathering vast historical and empirical data and

fitting them to various dynamical system frameworks consisting of covariant and interdependent explanatory variables. Although new models have been proposed throughout the years, certain challenges persist. A key obstacle is that the newer models frequently require ultrafast computing powers incurring increasingly steep and prohibitive costs to national and local governments. This challenge is particularly acute for developing countries in need of economic aid and disaster relief. Secondly, these new computation-heavy models may lack the atmospheric flexibilities unique to a region due to its specific topographies. Additionally, these costly models can be deficient at times in providing sufficient information that answers to the administrative tasks of energy consumption needs for its populations. Indeed, the cost-effective allocations of energy supplies in a region's smart energy grid are a perennial challenge to governments at all levels, national, regional, and local. Vast research has been directed to achieve efficiency in a region's energy grid given its specific climate patterns. For example, a recent research paper by Yilmaz studied the feasibility of generative adversarial networks (GANs) to improve energy efficiency by incorporating information and communication technologies in Türkiye energy grid [1]. The paper's author was able to demonstrate that trained synthetic load data are effective in reducing prediction errors in load when historical data and risk management calculations are combined. Putting these considerations together, the current paper examines the feasibility of harmonic oscillators as a basic principle in mid-term climate projections. The main objective and contribution of the current paper is that it gives a feasible, cost-effective model for median-term temperature projections with statistically tested accuracies well within the accepted margins of the scientific community. The paper is not the end, but the starting point in developing a cost-effective oscillation model with higher accuracy and provide certain general guidelines for future research in this direction.

The remainder of this section will review some popular regional climate models in detail. Section 2 will broaden the discussion to show the extensive applicability of harmonic oscillators in biology, chemical engineering, physics, and biochemistry. In Section 3, the paper gives the classical mechanics background and the basic atmospheric model. Section 4 furnishes the mathematical model with historical meteorological data in a region. Section 5 shows the statistical analyses of both the consistency and the predictive feasibility of the model, and finally, Section 6 gives an overview of future research directions.

Regional climate models are increasingly important in that they consider historical data unique to the locale and approach projections with the understanding that atmospheric behaviors at the global level cannot be reasonably construed as a summation of mesoscale regional ensembles. Different regional climate models coexist including Modele Atmospheric Regionale (MAR) developed by University of Grenoble in France, Advanced Regional Prediction System (ARPS) by University of Oklahoma, and Aire Limitée Adaptation Dynamique Développement International (ALADIN) developed and shared by 16 European and African countries. One particular advanced regional model that has gained notice is the Regional Atmospheric Modelling System (RAMS) by Colorado State University. With a projection scale of a few hundred square kilometers, RAMS utilizes the nonlinear finite-difference method fine-tuned by historical data to produce projections. The troposphere is divided into 3D grid intervals of equal volume Dq where q is a discretized stochastic variable. Time t is also considered as a discrete variable. Observations are made at discrete points in time $t_n = t_0 + nDt$ for $n = 0, 1, 2, 3, \ldots$, and Dt is the sampling time interval. The probability that the stochastic state variable q is in the volume grid i at time t_n is given by the relation $f_i(t_n)Dq$. Probability density function f at the next time interval t_{n+1} is given by the discretized sum of current states

$$f_i(t_{n+1}) = f_i(t_n) + \sum_{i'} D_i^{i'} f_{i'}(t_n). \tag{1}$$

In the above relation, $D_i^{i'}$ is the probability transition matrix from the i-th state to the i'-th state. The coefficients in the transition matrix satisfy $D_i^{i'} = W_i^{i'} - \delta_{ii'} \sum_p W_{i'}^p$, where $W_j^{k'}$ values are the transition coefficients updated in real-time by historical data in the recent past and normalized to conserved probability

$$\sum_{i'} W_i^{i'} = 1. \tag{2}$$

One challenge has been striking a balance between the desired resolution in the phase space on the one hand and the availability of computing resources and historical data on the other. Another challenge is that while the estimate of the transition improves with growing time series length, there is a threshold time series length beyond which forecast accuracies do not improve significantly. The RAMS climate projection system uses the HPE Cray supercomputer at 800 petaFlops to handle the ever-increasing need for vast computations. Other regional climate models such as MAR face even more challenges as different terrains and topographies across the Mediterranean require more variabilities to be incorporated into the computations, further straining government agencies' tight budgets in times of inflation, natural disasters, and energy supply disruptions. It is with these considerations, feasible and cost-effective mathematical models based on historical data become a focus of research.

2 Applicability of harmonic oscillators

A harmonic oscillator exemplifies the simplicity of the smooth transfer between kinetic energy and potential energy. The equation of the phase space of the harmonic oscillator is a second-order differential equation with initial values. The long-term asymptotic behaviors can be understood through the presence and the nature of damping in the system. Applications of harmonic oscillators abound in nearly all branches of natural, social, and behavioral science ranging from physics, biology, chemistry, ecology, economics, financial mathematics, and game theory to psychology. In ecology, Koshkin and Meyers showed recently in 2022 that a stressed predator-prey system can be modelled by harmonic oscillators where asymptotic limits can collapse into an attractor point in the Lotka-Volterra differential equation system [2]. Setting $x(t)$ and $y(t)$ to be the populations of the two species at time t respectively. The Lotka-Volterra system describes the interdependence between the prey population density $x(t)$ and the predator population density $y(t)$, respectively, as

$$\begin{aligned} \frac{dx}{dt} &= y(\alpha - \beta x), \\ \frac{dy}{dt} &= x(-\gamma + \delta y), \end{aligned} \tag{3}$$

where α, β, and γ are dynamical system constants and δ is a system parameter describing the species-specific covariance relation between prey's population and the growth rate of predator's population. Koshkin and Meyers defined the energy of the predator-prey harmonic oscillator system to be $V(x, y) \equiv x^2 + by^2$, where b is also a constant of the system. Each constant C represents an integral energy level of the predator-prey system

$$x^2 + by^2 = C. \tag{4}$$

The time derivatives of V along the trajectories of the system are given by

$$\dot{V}(x,y) \equiv \nabla V \bullet (\dot{x},\ \dot{y}) = \frac{\partial V}{\partial x}\dot{x} + \frac{\partial V}{\partial y}\dot{y}. \tag{5}$$

Denoting the point $(x(t), y(t))$ as $p(t)$ in the graph of two species, the Ω-limit is defined as the asymptotic behavior of the system

$$\omega_p \equiv \left\{ q \in \mathbb{R}^2 |\ p(t_k) \longrightarrow q \ as \ t \rightarrow \infty \right\}. \tag{6}$$

Koshkin and Meyers found that if environmental stress expressed as a damping coefficient $a > 0$ is present in the system, the derivative of the energy in the long-term limit is negative

$$\frac{d}{dt}V(x,y) = \frac{\partial V}{\partial x}\dot{x} + \ \frac{\partial V}{\partial y}\dot{y} = -2ax^2 < 0, \tag{7}$$

and the damped predator-prey oscillator system enters into a closed trajectory of energy ellipses and eventually collapses to a single-point Ω-limit q [2]. Harmonic oscillation also has numerous applications in chemical engineering, industrial engineering, and material science. In chemical engineering, certain cyclic hydrocarbon compounds such as benzene exhibits strong chemical stability due to the perfect symmetry in its six carbon-to-carbon and carbon-to-hydrogen covalent bonds. This stability of the benzene molecule causes intermolecular stacking to occur due to resonance delocalization of its electrons in the outer p atomic orbitals. The stable benzene molecule forms a double-deck crystalline structure in this type of intermolecular stacking whose noncovalent binding strength is modelled excellently by harmonic oscillators that utilize the periodic growth and decay of positive electrostatic potential on one benzene molecule relative to the negative electrostatic potential on the other benzene molecule in the above-described stacked structure. The electrostatic potential on a benzene molecule with resonance delocalization is given by the quantum harmonic potential

$$U(x) = \frac{1}{2}m\omega^2 x^2. \tag{8}$$

Here m is the molecular mass of benzene and ω is the angular frequency of the harmonic oscillation exhibited by the periodic increase and decrease in electrostatic potentials. In particular, the chemical stability of benzene due to the symmetry of its intra-molecular covalent bonds results in a slow evaporative property manifested by its distinct sweet aroma which is termed aromaticity in chemical engineering. The aromaticity of most cyclic hydrocarbon compounds is thus described excellently by a harmonic oscillation model with benzene as a reliable benchmark in industries. In a recent study, Arpa et al. [3] refined the harmonic oscillator model of aromaticity by reparametrizing the oscillation parameters of the classic carbon-to-carbon bond strength in acyclic hydrocarbon compounds ethane and ethylene. The researchers achieved the reparametrization of the harmonic oscillator model by approximating the aromaticity parameter α given as

$$\alpha = \frac{2}{\left(R_s - R_{opt}\right)^2 + \left(R_d - R_{opt}\right)^2}. \tag{9}$$

In Equation (9), R_s is the mean length of the pure single carbon-to-carbon bonds and R_d is the mean length of the pure double carbon-to-carbon bonds in ethane and ethylene and R_{opt} is the optimal carbon-to-carbon bond length in fully aromatic inert benzene experimentally measured to be 1.398-angstrom using neutron diffraction at 15 Kelvin. Thus, harmonic oscillator models are also important in chemical and industrial engineering research because these aromatic hydrocarbons are the backbone of industrial solvents, adhesives, plastics, and petrochemicals.

In quantum physics, harmonic oscillators are ubiquitous and are used extensively to model quantum phenomena. For example, Özdemir et al. [4] compared two types of computational bases in quantum entanglement. Denoting the initial state of an entangled system as ρ and the final state as ρ', the two states are related by a quantum phase operation $\mathcal{E} : \rho \to \mathcal{E}(\rho)$. One example of the quantum phase operation is the Kraus formalism given by

$$\mathcal{E}(\rho) = \sum_{\mu} E_{\mu} \rho\, E_{\mu}^{\dagger}. \tag{10}$$

The operator E_{μ} acts on the Hilbert space H_S of the entangled system and satisfies the completeness relation $\sum_{\mu} E_{\mu}^{\dagger} E_{\mu} = I$. Since a quantum system is never isolated and always interacts with its environment, the interaction introduces noise in quantum computation and information processing. This interaction is represented at time $t = 0$ in the entangled state as

$$\rho(0) = \rho_S(0) \otimes \rho_E(0). \tag{11}$$

The evolution of the time-dependent entangled system is given by

$$\rho(t) = U(t)\rho_S(0) \otimes \rho_E(0)U^{\dagger}(t), \tag{12}$$

where $U = e^{-iHt/\hbar}$. The Kraus representation of an entangled system is one where energy dissipation occurs via a damping process as a system interacts with its environment. Özdemir et al. [4] discovered that the Kraus representation for a single qubit whose computation basis is defined by the bosonic number states $\{\|0\rangle, \|1\rangle\}$ are given by the operators

$$
\begin{aligned}
A_0(t) &= |0\rangle \langle 0| + \sqrt{\eta}\, |1\rangle \langle 1|, \\
A_1(t) &= \sqrt{1-\eta}\, |0\rangle \langle 1|,
\end{aligned}
\tag{13}
$$

where $\sqrt{1-\eta}$ is the probability of the entangled system losing one qubit up to time t. The study compared the fidelities of the qubit states for the no-photon-decay event, the one-photon-decay event, and the two-photon-decay event. For example, it was discovered that the energy dissipation between the event of a one-photon-decay and two-photon decay up to time t, given as a damped harmonic oscillator with the above operator basis $\{A_i(t)\}$ exhibits a long-term fidelity behavior proportional to polynomial growths

$$\lim_{t \to \infty} F_1(t) - F_2(t) \propto \eta + \mathcal{O}\left[\eta^2\right]. \tag{14}$$

The harmonic oscillator has also found applications in biochemistry. For example, it is well-known that insulin and insulin-like growth factors 1 and 2, denoted as IGF1 and IGF2 have similar chemical structures. Although their precise mechanism of action is still unclear, it is known that these hormones activate two closely related receptor tyrosine-kinases called the insulin

receptor and IGF1 receptor respectively. Differences in the chemical kinetics of ligand binding and activations of receptors by insulin and IGF1 are generally thought to be the determining factors of their specificity. However, the receptors' ligand binding mechanisms show complex allosteric properties such as dependence on receptor disassociation rates. As a result, a more robust theory of receptor kinetics proved challenging for decades.

Kiselyov et al. [5] used harmonic oscillators to provide a valuable mathematical model for receptor kinetics. Using the concept that the active configuration of the receptors has higher free energy compared to that of the inactive configuration, Kiselyov et al. [5] modeled the behavior of the receptor mechanism near the point of activation as a harmonic oscillator. The idea is that separate subunits of the receptor are rigid bodies connected by covalent bonds similar to an elastic spring on a harmonic oscillator. In the model, the energy of the receptor oscillates harmonically when the receptor is in thermal equilibrium with the buffer. The energy of the receptor, as a result of random collisions with the buffer molecules, has a probability distribution given by the Maxwell formula

$$\frac{dP}{dE} = \frac{1}{KT}e^{-E/KT},$$ (15)

where P, E, and T are the probability, energy, and temperature of the ensemble, respectively, and k is the Boltzmann constant. The above distribution implies that the fraction of the insulin receptors having sufficient activation energy for binding is given by

$$\int_{E_{activation}}^{\infty} \frac{1}{KT}e^{-E/KT}dE.$$ (16)

By tagging select sites alternately with regular and radioactive binding ligands, De Meyts et al. [5] were able to theorize the binding reaction kinetics. For example, for sites 1 and 2 on the insulin receptors, the chemical equilibrium of the level of $r_{1\times2}$ is given by

$$r_{1\times2} = \frac{r_{tot}k_{cr}/(k_{cr}+d_2)}{1+\dfrac{d_1d_2}{a_1(k_{cr}+d_2)/L}},$$ (17)

where L *and* r_{tot} are the insulin concentration and total receptor levels respectively and the d_i's are the percentages of sites 1 and 2 remaining unbounded after insulin dissociation, k_{cr} is the critical kinetic constant, and a_1 is the dependence rate factor of site 1. Numerous other models of harmonic oscillators exist in natural science, behavioral science, and social science.

This paper is assembling a harmonic oscillator model of climate cycles with classic variables such as temperature. A word of caution is in order. In mathematical modelling, the current paper is fully aware that there exist explanatory models other than harmonic oscillators that can account for these natural phenomena. For example, in a recent paper, Mishra et al. [6] were able to combine the finite volume method and the Newton-Raphson method to study the calcium distribution across the membrane of a cholangiocyte cell and found that the diffusion rate follows a cutoff inverse sigmoid function. In addition, temperature itself can act with more complexity in natural phenomena that cannot be accounted for by a simple system of differential operators.

For example, in another recent study, Shah et al. [7] showed that temperature can cause convective flows across stratified surfaces in autocatalysis reactions in microorganisms. Thus, at times, a model based on these well-known mathematical frameworks alone is insufficient to provide explanatory power in studying some natural phenomena such as the movement of chemicals or

macro-particles across membranes or layers. At both the micro-level and the macro-level, natural phenomena can indeed exhibit more complexity than any simple but elegant mechanism alone can aptly capture. For example, the above-mentioned sigmoid saturation model, in contrast to a model of oscillators that shows periodicity, was successfully utilized as the activation function in a study of artificial intelligence-assisted detection methods of melanoma performed by Orhan and Yavşan [8]. In the study, the researchers chose the sigmoid function as the activation function in testing six classification algorithms' accuracy in melanoma detection models built on the convoluted neural network or CNN-based deep learning AI's. Among the six algorithms thus trained, the MobileNet algorithm achieved an accuracy rate of 89.4% in cancer detection [8]. In another study, Joshi et al. [9] considered a mathematical model that is framed to investigate the role of buffer and calcium concentration on fibroblast cells. Thus, future research should keep in mind that mathematical modelling of these natural or social phenomena may involve a multi-dimensional approach.

3 The classical harmonic oscillator

Harmonic oscillators are in essence the idealization of the continuous and reversible process of the transfer of kinetic energy into potential energy in a mass-spring system. The classical harmonic oscillator is best reified by the mass-spring system. The system has a natural equilibrium position where the mass and the restorative force of the spring are at static rest. Displacement of the mass away from the natural equilibrium position by a distance of x causes a restorative force F_1 proportional to the magnitude of the displacement and opposite in direction given by Hooke's law $F_1 = -kx$ where k is the spring constant. The force F_1 causes a potential energy $U(x)$ to be stored in the mass-spring system given by

$$U(x) = -\int_0^x F_1 du = \frac{k}{2}x^2. \tag{18}$$

Potential energy is continuously transferred to kinetic energy as the mass is moving from the stretched or compressed position to the equilibrium position. Denote the velocity of the mass as v, kinetic energy F_2 in the system with mass m at velocity v is given by $\frac{1}{2}mv^2$. By Newton's second law of motion, one obtains $F_2 = ma$. Since $a = \frac{d^2x}{dt^2}$, one has

$$F_2 = m\frac{d^2x}{dt^2}. \tag{19}$$

The conservation of energy means the sum of these two forces should be equal in magnitude and opposite in direction,

$$m\frac{d^2x}{dt^2} = -kx. \tag{20}$$

Normalizing both side by the mass m and re-writing $\frac{k}{m} = \omega^2$, where ω is the angular frequency, one has a linear second-order differential equation

$$\frac{d^2x}{dt^2} + \omega^2 x = 0. \tag{21}$$

The general solution of Eq. (17) giving the position x of the mass as a function of time t is

$$x(t) = Ae^{i\omega t} + Be^{-i\omega t}. \tag{22}$$

Using Euler's identity $e^{i\pi} = -1$, the above solution $x(t)$ can be rewritten in trigonometric terms. The period of motion is given by $T = \frac{2\pi}{\omega}$ and the frequency is given by $f = \frac{1}{T} = \frac{\omega}{2\pi}$. Should the system be subjected to damping, a positive damping constant β appears in the linear term $\frac{dx}{dt}$

$$\frac{d^2x}{dt^2} + \frac{\beta}{m}\frac{dx}{dt} + \omega^2 x = 0. \tag{23}$$

Setting $\frac{\beta}{m} = 2\lambda$, the damped case Eq. (19) further splits into three subcases according to the rates of deceleration given by the parity of $\lambda^2 - \omega^2$. For example, in the underdamped case where $\lambda^2 - \omega^2 < 0$, the solution becomes infinitely periodic and the oscillation flattens as $t \to \infty$

$$x(t) = e^{-\lambda t}\left[c_1 \sin\sqrt{\lambda^2 - \omega^2}t + c_2 \cos\sqrt{\lambda^2 - \omega^2}t\right]. \tag{24}$$

Overall, the free classical harmonic oscillator is an idealization of a perpetual motion machine in which energy exchanges forms without incurring any loss. In laboratories, retarding elements such as friction cause damping and eventually results in a cessation of periodic motion.

4 Basic Newton-Keplerian planetary model

The angular frequency ω in the harmonic oscillation relation Eq. (21) model is closely related to Kepler's laws of planetary motion and available astronomical data. Kepler's third law states that the ratio between the square of a planet's orbital period T and its semi-major axis a is constant within the solar system. Let M_s denote the mass of the Sun, m denote the mass of a planet, r be its mean distance from the star, and ω be the angular velocity. Since the gravitational force is balanced by the centrifugal force, Newton's law of universal gravitation means

$$mr\omega^2 = G\frac{M_s \bullet m}{r^2}. \tag{25}$$

Theorem 1 *The square of the period T is proportional to the cube of the mean distance from the star.*

Proof The angular frequency is defined as the mean angular speed measured in radians, thus one has

$$\omega = \frac{2\pi}{T}. \tag{26}$$

Squaring the above relation gives

$$\left[\frac{2\pi}{T}\right]^2 = G\frac{M_s}{r^3}. \tag{27}$$

Inverting the above relation, one has

$$\frac{r^3}{T^2} = G\frac{M_s}{4\pi^2}. \tag{28}$$

Since M_s and G are constants, one has the proportionality $T^2 \propto r^3$. This completes the proof.   ■

In most solar systems, the orbits of the planets around their stars are elliptical. Let a and b denote the semi-major and semi-minor axes of the two-body system respectively, then one has the following theorem:

Theorem 2 *The orbital period T is a function of both the semi-major and semi-minor axes a and b, respectively.*

Proof Since $M_s \gg m$, one can simplify the dynamics of the system as a two-body system with specific angular momentum $\mathbf{h}$ being the angular momentum $\mathbf{L}$ normalized by the mass of the planet, $\mathbf{h} = \frac{\mathbf{L}}{\mathbf{m}}$. Let $h = \|\mathbf{h}\|$. In a gravitationally bounded two-body system where the planet's displacement can be measured by angular movement, the infinitesimal operators of angle $d\theta$, time dt, and area dA are related as follows

$$
\begin{aligned}
dt &= \frac{r^2}{h}d\theta, \\
dA &= \frac{r^2}{2}d\theta.
\end{aligned}
\tag{29}
$$

Simplifying the differential operator relations above, one has $dt = \frac{2}{h}dA$. Further simplification leads to

$$
\frac{dA}{dt} = \frac{h}{2}.
\tag{30}
$$

Since h as the modulus of the mean normalized angular momentum specific to a planet-star system in question is a constant, this implies that the rate of change in the area swept out by the planet rotating around the star $\frac{dA}{dt}$ is also a constant, thus giving the Kepler's second law: the planet sweeps out equal areas in equal time. Performing a contour integration of the above identity over the full elliptical orbit of the planet to obtain the orbital period T, one has the following geometric identity relating the orbital period to the semi-major and minor axes and angular momentum:

$$
T = \oint dt = \oint \frac{2}{h}dA = \frac{2\pi ab}{h}.
$$

∎

In subsequent discussions, the mean angular displacement is denoted by $\overline{\omega}$ where $\overline{\omega} = \frac{T}{C}$ where the normalizing factor C is the cycle number in one complete orbital revolution. Additionally, the mean angular displacement is denoted by ω. With these notations, Kepler's second law states that ω is given by

$$
\omega = \frac{2\pi ab}{t\sqrt{p}\sqrt{M_s + m}},
\tag{31}
$$

where p is a parameter specific to the elliptical orbit of the two-body system related to the semi-major and semi-minor axes a and b by $p = \frac{b^2}{a}$ and t is the time for one orbit revolution. Normalizing the semi-major axis a to unity, the above relation reduces to $\frac{b}{\sqrt{p}} = 1$. Hence, Eq. (29) gives $\omega = \frac{2\pi}{t\sqrt{M_s + m}}$. Reducing the mass of the Sun to unity, one has $\omega = \frac{2\pi}{t\sqrt{1 + m}}$. Given the periodic nature of harmonic oscillators described above and the numerous applications across disciplines discussed in the last section, it is natural to infer that the cycles of seasonal changes such as annual cycles of monthly median temperature or lengths of daylight durations can also

be modelled by harmonic oscillations. Absent any sudden cosmic changes that adversely affect meteorological conditions such as monthly temperature, seasonal precipitations, or atmospheric pressure in a region, most data variables follow a periodic pattern within a year whose anomalies can be corrected by parametric statistics such as goodness of fit tests or analysis of variance tests. To that end, a rational model for monthly median temperature T in a region can be reasonably given by the coefficient-free harmonic oscillator

$$T(m) = \frac{iA}{2}\left[e^{-i\omega(m-c_1)} - e^{i\omega(m-c_1)}\right] + \frac{B}{2}\left[e^{i\omega(m-c_2)} + e^{-i\omega(m-c_2)}\right] + D. \tag{32}$$

In the above model, m is time given in months, the amplitude given by $\sqrt{A^2 + B^2}$ is modeled as an approximation of the difference between the highest monthly median temperature and the lowest monthly median temperature, the period of the oscillation is given by $\frac{2\pi}{\omega}$, and the undetermined coefficients c_i's are phase shifts and D is the vertical shift. Certain observations about a time-dependent atmospheric dynamics model are worthy of mention. First, since meteorology variables in shorter time intervals exhibit more random behaviors, the longer interval of months is used. Hence, there arises the consideration of which method of time-keeping should be utilized, be it the lunar calendar or other types. Second, once a particular method of time-keeping is selected, there is the additional consideration of the uneven residue of the orbital period of the Earth around the Sun and how the residue is accounted for in the model. Third, there is also the consideration of the axial precession of the Earth.

Table 1. Monthly median temperatures of New York City from July 2017 to July 2021

2017		2018		2019		2020		2021	
Month	Temperature	Month	Temperature	Month	Temperature	Month	Temperature	Month	Temperature
		Jan	-1	Jan	0.5	Jan	3.5	Jan	2
		Feb	5.5	Feb	2.5	Feb	4.5	Feb	1
		Mar	5	Mar	6	Mar	8	Mar	7.5
		Apr	10	Apr	13.5	Apr	10	Apr	12.5
		May	19.5	May	17	May	16	May	17.5
		Jun	22.5	Jun	22	Jun	22.5	Jun	23
Jul	24	Jul	26.5	Jul	26.5	Jul	26.6	Jul	24
Aug	23	Aug	26	Aug	23.5	Aug	25		
Sept	20.5	Sept	21.5	Sept	21	Sept	20		
Oct	17.5	Oct	14	Oct	15.5	Oct	13.5		
Nov	8	Nov	7	Nov	6.5	Nov	11.7		
Dec	2	Dec	3.5	Dec	3.5	Dec	3.5		

The precession is caused by the westward movements of the equinoxes along the ecliptic relative to visually fixed stars in the heavens. Although the axial precession has a period of approximately 25,798 years, the choice of longer time variables can introduce anomalies in the model. There exist other considerations in addition to the ones mentioned above. The harmonic oscillator model at present is one among a whole set of mathematical models utilized to understand the complexity of atmospheric dynamics. Hence, the parameters of the model can and should be improved as more accurate data become available. In the present discussion, the monthly median temperature in New York City is utilized. These monthly median temperatures were collected from July 2017 to July 2021 available on public domains [10]. It should be stressed that different public domains may post slightly different monthly median temperatures for the same region. The above temperatures are monthly median temperatures. Observe that the median temperatures

above exhibit sinusoidal wave patterns with maximum between the months of June and August of each year and minimum between the months of December and February. A connected scatterplot in Excel was used to visualize these data points. To further visualize the data, the months were coded with the first month, July of 2017 as 7 and each subsequent month having an increment of 1, thus converting categorical data into ordinal-numeric data ready for modeling and parametric statistical analysis. Notice in the scatterplot, a rapid increase in median temperatures between
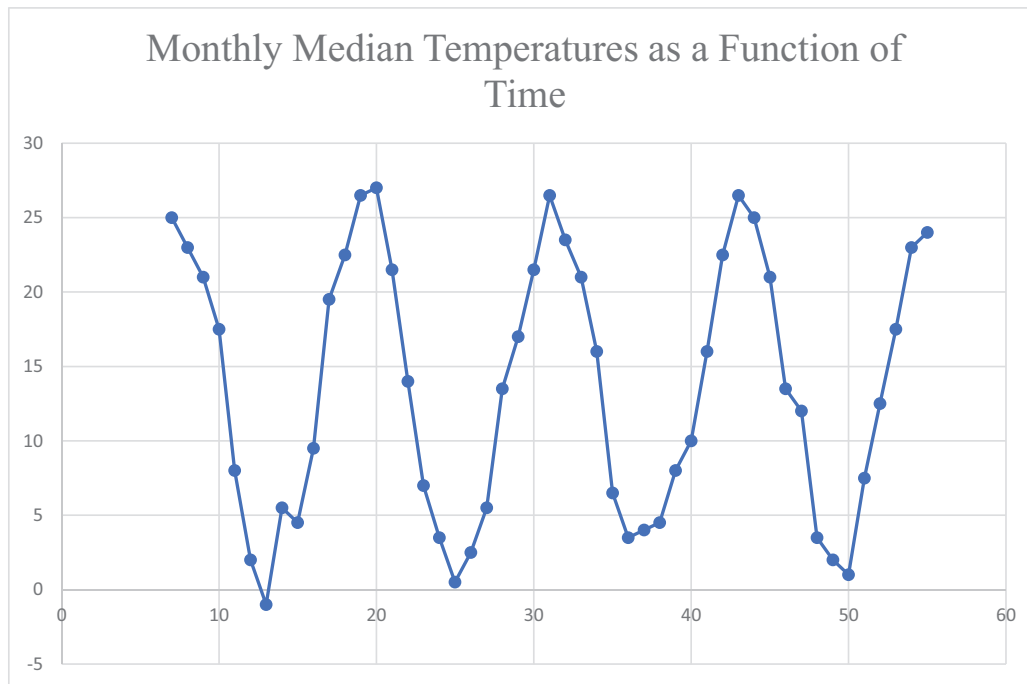
Figure 1. Connected scatterplot of monthly median temperatures of New York City

$5°$ and $20°$ spanned three months out of a year. These three months are typically March, April, and May in the spring. Conversely, a rapid decrease in median temperatures between $21°$ and $7°$ also spanned three months out of a year. These three months are typically September, October, and November in the fall. Also notice that the change in temperature between December of a year through February of the following year is usually less than $6°$ in general. This latter pattern was also exhibited in the three-month period between June and August of a year. For example, in the year 2019, the median temperatures in June, July and August were $21.5°$, $26.5°$, and $23.5°$ respectively. This indicates a temperature increase of only $5°$ in the three-month period in 2019.

This sequential pattern of rapid temperature increases between March, April, and May, followed by a period of minimal change, and the subsequent rapid decrease in September, October, and November which is turn followed by a period of minimal change in December, January, and February coincides well with that of a classical harmonic oscillator. Recall in the harmonic oscillator, the mass moves rapidly as it crosses the equilibrium position and moves slowly when the mass is close to the overstretched or over-compressed positions. Relation (26) gives a workable model of mean angular displacement per unit of time calculated in earth days as $\omega = 0.01720209895 \ radians/day$. In the current model, if one were to use months to minimize the effects of random meteorological anomalies, setting the uneven monthly residue to zero gives $\omega = 0.516062969 \ radians/month$. Allowing for 31 days in a month gives a higher monthly angular displacement of $\omega = 0.533365067 \ radians/month$. To optimize the monthly median temperatures specific to New York City from July, 2017 to July 2021, the intermediate value $\omega = 0.523598776$

was used for the model. In the next section, a visual proximity test was conducted and a parametric statistical test was also conducted to see how closely optimize the actual data. Thus, based on the available data, a harmonic oscillator model of the monthly median temperature T as a function of time measured in month m in New York City from July 2017 to July 2021 can be given as

$$T(m) = \frac{8.95}{2}[(1+i)e^{-0.523598776i(m-5.5)} + (1-i)e^{0.523598776i(m-5.5)}] + 13.4. \tag{33}$$

In this region-specific model, it is assumed that the phase angle $\phi = \tan^{-1}\left[\frac{A}{B}\right]$ is $\frac{\pi}{4}$ radians, thus setting $A = B$ in the coefficient-free oscillator in Eq. (30). The magnitude of the amplitude is modelled by trimmed minimum of the data set with the extreme cold month of January 2018 removed. Thus, the difference between the maximum and trimmed minimum is $26.6\text{L}' - 0.5\text{L}' = 26.1\text{L}'$ with an observed difference of $\frac{26.1\text{L}'}{2} \cong 13.1\text{L}'$. To fit the data sufficiently, the model utilized an amplitude of

$$\sqrt{A^2 + B^2} = \sqrt{8.95^2 + 8.95^2} \cong 12.7\text{L}' \tag{34}$$

whose difference is comfortably within 97% of the observed amplitude.

5   Numerical simulations and statistical analysis of the model

To test how closely the harmonic oscillator model approximates the actual data. A visual proximity test by superimposing the predicted temperatures and the actual data on the same graph shows the feasibility of the harmonic oscillator model trained on actual data when sufficient data were utilized as training data.
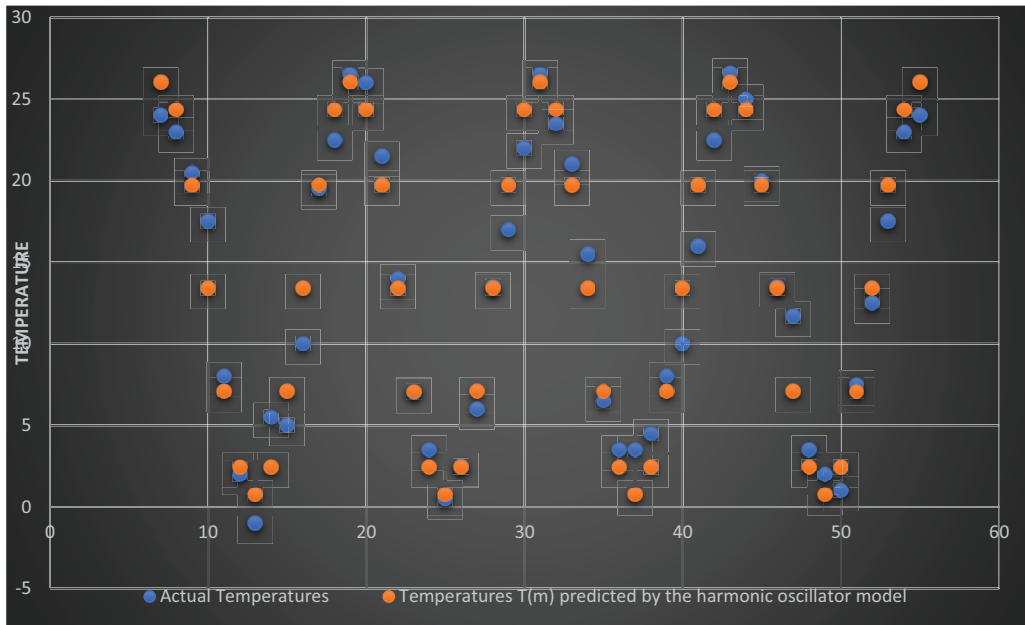
Figure 2. Comparison of monthly median temperatures of New York City compared to predicted by the harmonic oscillator model

Notice that in the overstretched and over-compressed regions in the visual proximity graph, the model's predicted temperatures $T(m)$ given as orange points approximate the actual temperature data given as blue dots well. In the equilibrium position, some variations can be observed.

For example, in October of 2017, the predicted median temperature was 13.399° and the actual recorded temperature was 17.5°. This pair constitutes the pair with the largest deviation. During the other months near the equilibrium point, the deviations were visibly smaller.

To complete the statistical analysis, a goodness of fit test was utilized to examine the predictive power of the harmonic oscillator model. The goodness of fit test is a parametric test that measures the deviation of the data points E expected by a hypothesized model and the actually observed field data O using the χ^2 distribution. The test statistic is given by

$$\chi^2 = \sum \frac{(O - E)^2}{E}. \tag{35}$$

For example, for the months between July 2017 and January 2018, the observed monthly median temperatures and the expected monthly median temperatures are given in the following table of partial results.

Table 2. Partial observed vs. predicted monthly temperatures of New York City

Year	Coded Month	Observed Temperature O	Expected Temperature E	O - E	$\frac{(O\text{-}E)^2}{E}$
2017	7	24	26.0572	-2.0572	0.1624
	8	23	24.3615	1.3615	0.0761
	9	20.5	19.7286	0.7714	0.0302
	10	17.5	13.4	4.1	1.2545
	11	8	7.0714	0.9286	0.1219
	12	2	2.4385	-0.4385	0.0789
2018	13	-1	0.7428	-1.7428	4.0891

Recall that the χ^2 distribution is a right-skewed distribution and that the goodness of fit test based on the χ^2 distribution is premised on the null hypothesis that the observed values are close to the expected values predicted by the model. Thus, at a preset significance level, one rejects the null hypothesis if the χ^2 the test statistic is high, implying significant deviations between the observed and the predicted values. Conversely, a low test statistic fails to reject, implying the observed values and the predicted values are statistically and sufficiently close not to warrant a rejection at the preset significance level.

With a degree of freedom at $k - 1 = 48$, at $\alpha = 0.10$ significance level, the χ^2 test fails to detect significant statistical differences between the actual monthly median temperatures and the predicted monthly median temperatures by the model at 90% confidence level demonstrating the consistency of the model. To further test the consistency of the model, the author put the model to the test with higher statistical rigor at the $\alpha = 0.05$ significance level. The test statistic is 34.7312 with a p-value above the null hypothesis rejection level again. Thus, both goodness of fit statistical tests failed to detect significant statistical differences between the actual monthly median temperatures and the predicted monthly median temperatures by the model at the 90% and 95% confidence levels. In addition to consistency, goodness of fit tests were also performed on historical data entirely outside of the training data used in the construction of the model in order to test the model's predictive power. Actual observed monthly median temperatures in New York City in the 12-month period from August, 2021 to July 2022 from the same public domain were statistically compared with model's predicted temperature at both the $\alpha = 0.05$ significance level and the $\alpha = 0.01$ significance level. At both significance levels, the goodness of fit test gave an F-ratio of 0.0605 and could not detect statistically significant differences between the

predicted median monthly temperature and the observed median temperature thereby supporting the predictive power of the cost-effective harmonic oscillation model.

6 Discussion and further research directions

The current research gives a vantage point to investigate the feasibility of using harmonic oscillators to model atmospheric dynamics, thus opening the possibilities in forecasting energy consumption and other areas of public policy related to climate science. Natural questions include but are not limited to in what ways can the model be improved; should damping be present in the model; if so, what are the causes of damping; what mechanism should be used in the model to account for axial precession of Earth, and can the same approach be utilized to analyze periodic cycles of annual precipitation. Numerous other questions and considerations exist in this direction. As such, the current paper is a starting point. This section will first discuss certain climate-specific research directions in the future, then it will broaden the discussion to include certain philosophical implications in the generalized harmonic oscillator model going forward. Based on the research presented, a possible area of future research to refine the current harmonic oscillator model is to fine-tune the mid-term monthly model by incorporating fluid dynamics with fractional calculus. In many areas of applied mathematics, fractional calculus has increasingly proved to hold explanatory power. For example, Ahmed et al. [11] have recently discovered a fractional calculus model using Caputo-Fabrizio fractional-order PDE to study the evolution of the cholera epidemic. The model thus derived contained a system composed of four fractional differential equations with input variables such as size of susceptible population and symptomatic infected population. Moreover, a theorem of the uniqueness and existence of solutions to the Caputo-Fabrizio fractional-order cholera model was also found. In atmospheric science, it is well-established that shorter-term atmospheric behaviors such as weekly median temperature or weekly precipitation in extreme weather conditions such as hurricanes can be modeled more accurately by hydrodynamic ensembles. For example, a hurricane is a moving frame of low hydrodynamic depressions with high atmospheric convection and an enclosed equatorial atmospheric circulation spreading to higher latitudes. In the analysis of these lower-than-mid-term projections, turbulent fluids in the hurricane column such as air or water vapors observe fractional conservation of mass in hydrodynamic behaviors given by

$$-\frac{\partial^\alpha \rho q_i}{\partial x_i^\alpha} = \frac{\Gamma(\alpha+1)}{\acute{x}^{\alpha+2}} \frac{\partial}{\partial t}\left(\acute{x}^3 n\rho\right). \tag{36}$$

In the above equation, the standard control volume's 3D lengths are given as $\acute{x}_i$ for $i = 1, 2, 3, \rho$ is the mean air/water vapor density, q_i is the specific hydrodynamic discharge passing through the i-th face of the standard control volume, $\Gamma(\alpha+1)$ is the gamma function, n is the porosity parameter of the air/water vapor mixture, and $\frac{\partial^\alpha}{\partial x_i^\alpha}$ is the α-th fractional derivative.

For example, Wheatcraft et al. [12] were able to utilize the above fractional calculus relation to study non-linear hydrodynamic flux in control volumes. The research showed that the hydrodynamic divergence term in the fractional mass conservation equation is the fractional convergence and that the scaling term in the fractional conservation of mass is in fact scale-invariant. Combining these latter considerations together with the research presented in the current paper, a more comprehensive mid-term or short-to-mid-term atmospheric model can be reasonably given by a system of both differential and fractional differential equations in which the master harmonic oscillator model first gives the overall projections, then the fractional derivative transient model modifies the above macro projections with more short-term refinement.

Another further research direction is to consider the philosophical nature of physical variables

present in the model. For example, is the meaning of mass m used in the definition of angular frequency ω limited to the total mass of the gravitationally bound two-body problem consisting of Sun and Earth with the negligible mass of the Moon absorbed into the approximation for computation purposes or are there more generalized epistemological ensembles that can account for harmonic oscillations in these vastly disparate natural and social phenomenological settings. This is a particularly important direction of future research based on the presented results. A review of the literature on the applications of the harmonic oscillator in natural sciences and social sciences shows that the meaning of the modelled variables can have discipline-specific interpretations in some cases while eludes satisfactory interpretations in others. For example, an application of the harmonic oscillator where the authors gave a plausible interpretation of the meaning of the modelled variables is a quantum spatial-periodic harmonic model of equity market with price limits by Meng et al. [13]. The authors of the study examined the price action movement of equities modelled as a fundamental particle moving, vibrating, and undergoing excitations in a quantum potential well with energy given as

$$V(x) = \frac{m\omega^2 x^2}{2}. \tag{37}$$

The authors reasoned that the energy band structures of the quantum harmonic oscillator model correspond to the non-linear market relations such as inter-band positive correlations and intra-band negative correlations between volatility and the transaction volume in unit time. The probability of locating the equity at price x modelled as the statistical location of the fundamental particle is given as the square modulus of the generalized Schrodinger wave function with a duly coupled Gaussian

$$|\varphi(x)|^2 = \sqrt{\frac{m\omega}{\pi\hbar}} e^{-m\omega x^2/\hbar}. \tag{38}$$

The authors posited that the modelled variables m, ω, $\hbar$ are interpreted as the mean total market capitalization of the equity, period of the equity fluctuation cycles, and most importantly the uncertainty of the irrational transaction volume of the equity respectively. To fit the model with a market circuit where trading is halted in the presence of extreme equity valuation volatilities, the authors further imposed a periodic boundary condition when the price exceeds \$d above the mean daily moving average or drops \$d below the identical mean daily moving average given as

$$\varphi(x) = e^{-ikd}\varphi(x+d). \tag{39}$$

where k is the one-dimensional Bloch wave number. With the market circuit thus modelled, the price of the equity is given as

$$\varphi(\xi) = e^{-\frac{\xi^2}{2}} \left[A \bullet H_1(\xi) + B \bullet H_2(\xi) \right]. \tag{40}$$

where H_i's are the first and the second Hermite polynomials and the parameters A and B are the constants specific to the equity in consideration. Thus modelled, the authors were able to obtain the solution of the equity wave function in Eq. (38) as

$$\left[H_1\left(\frac{-\beta d}{2}\right) - e^{-ikd} H_1\left(\frac{\beta d}{2}\right) \right] \bullet \left[H_2'\left(\frac{-\beta d}{2}\right) - e^{-ikd} H_2'\left(\frac{\beta d}{2}\right) + \beta d e^{-ikd} H_2\left(\frac{\beta d}{2}\right) \right], \tag{41}$$

where β is a re-parametrization constant coupling the price of the equity to ξ

$$\xi = \beta x = \sqrt{m\omega/\hbar \bullet}x. \tag{42}$$

It is worthy of consideration to note that the authors further inferred from the model that the reduced Planck constant $\hbar$ is the limit of irrational agency in equity trading, that is, in the perfectly rational market, $\hbar \to 0$.

One can ask: in the limit, is the efficient market hypothesis or EMH tenable? If financial information is made transparent, symmetric, and accessible to all market participants such as to all institutional investors and individual investors, can the rational market be a frictionless harmonic oscillator where the only uncertainty is the most natural quantum price fluctuations captured by a geometric Brownian motion X_t?

$$\varphi(\xi) \cong Ae^{i\xi t} + Be^{-i\xi t} + X_t. \tag{43}$$

If these conditions are tenable, then the logarithmic price of an equity P_t at time t is a simple linear sum of the expected value of the equity E_t and the stochastic discount factor M_t

$$\log P_{t+1} \;=\; \log M_t + E_t \bullet \log P_t. \tag{44}$$

A natural question is: what would a rational trading strategy be in the stated limit? These and other long-term considerations should be investigated by the mathematical modelling community.

Declarations

List of abbreviations

Not applicable.

Ethical approval

The author states that this research complies with ethical standards. This research does not involve either human participants or animals.

Consent for publication

Not applicable.

Conflicts of interest

The author confirms that there is no competing interest in this study.

Data availability statement

Data availability is not applicable to this article as no new data were created or analysed in this study.

Funding

Not applicable.

Author's contributions

The author has made substantial contributions to the conception, and design of the work, the acquisition, analysis, interpretation of data, and the creation of new software used in the work.

References

[1] Yilmaz, B. Generative adversarial network for load data generation: Tükiye energy market case. *Mathematical Modelling and Numerical Simulation with Applications*, 3(2),141-158, (2023). [CrossRef]

[2] Koshkin, S. and Meyers, I. Harmonic oscillators of mathematical biology: many faces of a predator-prey model. *Mathematics Magazine,* 95(3), 172-187, (2022). [CrossRef]

[3] Arpa, E.M. and Durbeej, B. HOMER: a reparameterization of the harmonic oscillator model of aromaticity (HOMA) for excited states. *Physical Chemistry and Chemical Physics*, 4(25), 95-127, (2023). [CrossRef]

[4] Özdemir, Ş.K., Liu Y., Miranowicz, A. and Imoto, N. Kraus representation of a damped harmonic oscillator and its application. *Physical Review A,* 70(4), 54-92, (2004). [CrossRef]

[5] Kiselyov, V.V., Versteyhe, S., Gauguin, L. and De Meyts, P. Harmonic oscillator model of the insulin and IGF1 receptors' allosteric binding and activation. *Molecular Systems Biology*, 5(243), 773-806, (2009). [CrossRef]

[6] Mishra, V., Nakul, N. and Adlakha, N. Finite volume simulation of calcium distribution in a cholangiocyte cell. *Mathematical Modelling and Numerical Simulation with Applications*, 3(1), 17-32, (2023). [CrossRef]

[7] Shah, N.A., Popoola, A.O., Oreyeni, T., Omokhuale, E. and Altine, M.M. A modelling of bioconvective flow existing with tiny particles and quartic autocatalysis reaction across stratified upper horizontal surface of a paraboloid of revolution. *Mathematical Modelling and Numerical Simulation with Applications,* 3(1), 74-100, (2023). [CrossRef]

[8] Orhan, H. and Yavsan, E. Artificial intelligence-assisted detection model for melanoma diagnosis using deep learning techniques. *Mathematical Modelling and Numerical Simulation with Applications,* 3(2),159-169, (2023). [CrossRef]

[9] Joshi, H., Yavuz, M. and Stamova, I. Analysis of the disturbance effect in intracellular calcium dynamic on fibroblast cells with an exponential kernel law. *Bulletin of Biomathematics,* 1(1), 24-39, (2023). [CrossRef]

[10] Current Results weather and science facts. New York City Temperatures: Averages by Month *https://www.currentresults.com/Weather/NewYork/Places/new-york-city-temperatures-by-month-average.php,* Access Date: 25th April 2023.

[11] Ahmed, I., Akgül, A., Jarad, F., Kumam, P., and Nonlaopon, K. A Caputo-Fabrizio fractional-order cholera model and its sensitivity analysis. *Mathematical Modelling and Numerical Simulations with Applications,* 3(2), 170-187, (2023). [CrossRef]

[12] Wheatcraft, S.W. and Meerschaert, M.M. Fractional conservation of mass. *Advances in Water Resources*, 31(10), 1377-1381, (2008). [CrossRef]

[13] Meng, X., Zhang, J.W., Xu, J. and Guo, H. Quantum spatial-periodic harmonic model for daily price-limited stock markets. *Physica A: Statistical Mechanics and its Applications,* 438, 154-160, (2015). [CrossRef]

Mathematical Modelling and Numerical Simulation with Applications (MMNSA)
(https://dergipark.org.tr/en/pub/mmnsa)